promoting access to White Rose research papers

White Rose Research Online

Universities of Leeds, Sheffield and York
http://eprints.whiterose.ac.uk/

This is an author produced version of a paper published in **Combustion and Flame.**

White Rose Research Online URL for this paper:

http://eprints.whiterose.ac.uk/77764/

Paper:
Bradley, D, Lawes, M and Mansour, MS (2009) *Explosion bomb measurements of ethanol-air laminar gaseous flame characteristics at pressures up to 1.4 MPa.* Combustion and Flame, 156 (7). 1462 - 1470.

http://dx.doi.org/10.1016/j.combustflame.2009.02.0...

White Rose Research Online
eprints@whiterose.ac.uk

Explosion Bomb Measurements of Ethanol-air Laminar Gaseous Flame Characteristics at Pressures up to 1.4 MPa.

D. Bradley, M. Lawes and M. S. Mansour

School of Mechanical Engineering, University of Leeds, Leeds LS2 9JT

Full length article

Corresponding author: D. Bradley Tel. --113 343 2115 Fax --113 343 2150

e-mail: d.bradley@leeds.ac.uk

Keywords: Ethanol burning velocities, Markstein numbers, critical flame instability data, explosions

Shortened title: "Ethanol-air Laminar Flame Characteristics up to 1.4 MPa."

Abstract

The principal burning characteristics of a laminar flame comprise the fuel vapour pressure the laminar burning velocity, ignition delay times, Markstein numbers for strain rate and curvature, the stretch rates for the onset of flame instabilities and of flame extinction for different mixtures. With the exception of ignition delay times, measurements of these are reported and discussed for ethanol-air mixtures. The measurements were in a spherical explosion bomb, with central ignition, in the regime of a developed stable, flame between that of an under or over-driven ignition and that of an unstable flame. Pressures ranged from 0.1 to 1.4 MPa, temperatures from 300 to 393K, and equivalence ratios were between 0.7 and 1.5. It was important to ensure the relatively large volume of ethanol in rich mixtures at high pressures was fully evaporated. The maximum pressure for the measurements was the highest compatible with the maximum safe working pressure of the bomb. Many of the flames soon became unstable, due to Darrieus-Landau and thermo-diffusive instabilities. This effect increased with pressure and the flame wrinkling arising from the instabilities enhanced the flame speed. Both the critical Peclet number and the, more rational, associated critical Karlovitz stretch factor were evaluated at the onset of the instability. With increasing pressure, the onset of flame instability occurred earlier. The measured values of burning velocity are expressed in terms of their variations with temperature and pressure, and these are compared with those obtained by other researchers. Some comparisons are made with the corresponding properties for iso-octane-air mixtures.

1. Introduction

Ethanol is an important engine bio-fuel, either alone, or in a carefully selected fuel blend, yet there are only limited measured data of its characteristics at operational pressures. It has somewhat similar stoichiometric laminar burning velocities to gasolines, but a greater resistance to engine knock. Measurements in a counter-flow burner with fuel-lean mixtures show it to have a higher extinction strain rate than iso-octane [1]. This is advantageous in reducing localised flame extinctions and re-ignitions in highly turbulent flames [2]. Its disadvantages are that it is hygroscopic (with consequent effects on vapour pressure), can corrode light metals, has a lower vapour pressure than gasoline, a smaller liquid volumetric energy, and a higher latent heat of vaporisation [3]. The lower vapour pressure reduces "startability" in port fuel-injected engines. However, it is suggested in [4] that the vapour pressure of ethanol-gasoline blends can be increased above that of gasoline alone if the mole percentage of gasoline in the blend exceeds about 35, at 311K. The same stoichiometry necessitates higher fuelling rates. In supercharged engines some of the fuel can be injected into a supercharger inlet, where its enhanced cooling effect, due to the higher latent heat of vaporisation, improves compressor efficiency, as well as increasing the inhaled energy [3]. The cooling from vaporisation also enhances knock resistance [5].

Currently, with the increasing range of possible suitable fuels and their blends for engines, it is necessary to specify the associated combustion characteristics, over the full range of equivalence ratios. These cover vapour pressure, laminar burning velocity, Markstein numbers, ignition delay times, excitation times, stretch rates for the onset of flame instabilities and also for flame extinction. In conjunction with blending laws, which are usually non-linear, knowledge of these characteristics is necessary for the design of fuels appropriate to different engines and energy conservation strategies. For contemporary engine designs the expression of knock ratings by Research and Motor Octane numbers is only relevant to a rather narrow operational range of pressure and temperature [6]. Ignition delay data are more directly relevant, and are now becoming available over a wider range of pressure and temperature for different fuels.

The present measurements extend the ranges of data for ethanol-air mixtures on laminar burning velocities, Markstein numbers and critical Karlovitz stretch factors for the onset of flame instabilities and for flame extinction to higher pressures. Flame speeds, flame radii, and pressures were measured during spherical explosions in a spherical bomb, over the full range of equivalence ratios and all data were derived from these.

Previously, Gülder [7] has obtained laminar burning velocities, u_ℓ, of ethanol–air mixtures up to 0.8 MPa pressure and up to 500K, over a wide range of equivalence ratios, ϕ. These were derived from flame speed measurements during the constant pressure period of combustion in a spherical bomb. Egolfopoulos et al. [8] have measured ethanol-air burning velocities at atmospheric pressure and temperatures ranging between 363 and 453K in counter-flow flames, over a full range of ϕ. More recently, Liao et al. [9] have used schlieren photography measurements during explosive combustion at constant pressure in a cylindrical bomb, at 0.1 MPa and at temperatures between 358 and 480K, to obtain u_ℓ over a wide range of ϕ. Chemical kinetic models have predicted values of u_ℓ and, for lean mixtures, extinction strain rates [8, 10]. These were, respectively, higher and lower, than those measured [1]. The chemical kinetic modelling of Marinov [10] embraced both laminar burning velocities and ignition delay times over a full range of mixtures of ethanol-air.

For the spherical explosion technique, the different algebraic expressions for the burning velocity, involving flame radius, *r*, pressure, *p*, and time, *t*, have been presented in [11]. Allowance must be made for the effects of the flame stretch rate, α, given by $(1/A)(dA/dt)$, where *A* is the flame surface area. For a spherical flame, this gives:

$$\alpha = (2/r)S_n, \tag{1}$$

where $S_n = dr/dt$, the flame speed.

In reality, α is the sum of the aerodynamic flame strain rate, α_S, and the stretch due to flame curvature, α_c, the expressions for which are given in [12]. For established stable flames there is a linear relationship between S_n and α. The associated Markstein numbers, Ma_{sr} and Ma_{cr}, are obtained from the changes in the stretched flame burning velocity with α_S and α_c [12]. This approach was used in [13, 14], but the onset of Darrieus-Landau and thermo-diffusive instabilities at lower stretch rates destroys the linear relationship. The instabilities wrinkle the flame, with an associated increase in burning velocity [13-15]. The transition to an unstable flame occurs at a critical value of the Peclet number, Pe_{cl}, the critical flame radius, r_{cl}, normalised by the flame thickness, δ_ℓ, here taken to be ν/u_ℓ, where ν is the kinematic viscosity of the mixture. More fundamentally, this is associated with the laminar Karlovitz stretch factor, K_ℓ, given by $\alpha\delta_\ell/u_\ell$, falling to a critical value, K_{cl}, below which

the flame becomes unstable [16]. All these parameters were measured in the course of the present study.

The measurements were most conveniently made with central ignition during the earlier, higher stretch rate, regime of constant pressure combustion. The aim was to obtain data up to the highest possible pressures. The limiting maximum pressure is set by the maximum safe design pressure of the bomb. Measurements during the initial combustion at constant pressure are inevitably at a pressure well below the maximum pressure attained in the explosion. To make measurements at the higher pressures, flame propagation must be recorded in the final stage of burning. With windows orientated to view the central region of the bomb, this can be achieved with twin ignitions at opposed points on the inner surface of the bomb and flames propagating towards the centre of the bomb [17]. However, Markstein and critical Peclet numbers are not so conveniently obtained under these lower stretch rate conditions, and allowance must be made for the increased flame speeds due to instabilities.

The present paper describes the derivation of the data from measurements during the early, constant pressure, stage of combustion in a spherical explosion bomb, with central ignition. Measurements were at higher pressures than have been made previously, of up to 1.4 MPa, with values of ϕ between 0.7 and 1.5. The values of u_ℓ are compared with those from experiments in [8, 9] at 0.1 MPa, and those in [7] at up to 0.8 MPa. The last had no allowance for stretch rate effects. Comparisons also are made with the computed values in [8] and [10]. Limitations can arise, and have arisen in the past, from the vapour pressure being insufficient to attain an entirely gas phase mixture, and these are discussed. Markstein numbers for strain rate and curvature are presented; the latter were derived indirectly as in the past, and the limitations of this are discussed. Most of the flames eventually became unstable, at a radius that decreased with increase in pressure. Measurements were made only in the regime of stable flames, which lay between those of under or over-driven ignition at high stretch rates and of instabilities at low stretch rates. These limits had first to be identified. The critical Peclet number was found at which flames became unstable, but it is proposed that a critical Karlovitz factor is a more fundamental parameter and values of this are presented. More tentatively, a technique is suggested for deriving extinction stretch rates from explosion flame data.

2. Experimental method

The spherical stainless steel bomb employed had three pairs of orthogonal windows of 150 mm diameter and has been described in [13]. The internal radius of the bomb, *R*, and that of a

sphere with the same internal volume as the bomb, R_0, were 190 mm and 192.8 mm, respectively. The bomb and mixture were heated up to 395K by a 6 kW electric heater, located at the wall, and the initial gas temperature was measured with a sheathed chromel-alumel thermocouple. Four fans, driven by electric motors, located close to the wall of the bomb initially mixed the reactants. It was vital to ensure all the liquid was evaporated and the fans were important in enhancing heat transfer from the heater surface.

The volume of ethanol to be injected into the bomb was found from the required mole composition, the liquid ethanol density, and the known volume of the bomb. Because of the ethanol-air stoichiometry, the amount of liquid fuel injected, which was of 99.8% purity, was quite large. It was injected with a Gas Tight syringe, through a needle valve. Four syringes were employed, with volumes of 5, 10, 25 and 50 cm^3, depending upon the volume of fuel required. The largest volume of ethanol introduced was 52.72 cm^3 at ϕ = 1.4 and 1.0 MPa, at 358 K. Injection occurred with the air in the bomb at a pressure of about 0.05 MPa. Further dried air was introduced and the value of ϕ found by the method of partial pressures. As ϕ increased at the higher pressures, more time was required to evaporate the fuel, up to a maximum of three minutes for ϕ = 1.4 at 1.0 MPa. The measured partial pressures indicated when evaporation was complete. The gas phase temperature decreased during evaporation, then returned to the initial temperature. A Kistler pressure transducer measured pressures during the explosion. A central spark plug with ignition energies of about 23 mJ, was supplied from a 12 V transistorised automotive ignition coil. At a temperature of 300K rather more energy was required and this was supplied by a variable high energy ignition unit.

Flame images were captured, by schlieren cine photography, to obtain flame speeds, stretch rates and Pe_{cl}. A high speed Phantom digital camera with 256 megabytes integral image memory was used. The camera speed was 2,000 frames/s with 768 x 768 pixels and the resolution was 0.223 mm/pixel. Three explosions were performed and complete data sets obtained for each separate condition. For each explosion mean flame radii, obtained from measurements of the projected flame area were plotted against time. Flame speeds were found by numerical differentiation, using central differencing with five closely spaced radii. Values usually agreed within a total scatter of 1.2 %. The principal uncertainty was in making up the mixture. Analysis showed that the uncertainty in ϕ could range from 1.0% at ϕ =1.4 and 0.5 MPa, up to a maximum of 3% at ϕ =0.7 and 0.1 MPa. The average uncertainty over all explosions was 1.4%. At higher pressures the restricted range of stable flame measurements increased the uncertainty in values of both u_ℓ and the Markstein numbers.

Changes in the measured flame speed, S_n, with flame radius, obtained from flame image analyses for explosions at ϕ = 0.9, a temperature, T_u, of 358K, and pressures of 0.1, 0.7 and 1.2 MPa are shown in Fig. 1. Figure 2 shows the similar relationships for ϕ = 1.2 at 0.1, 0.5 and 1.0 MPa, again at 358K. Four of the six flame speeds in the two figures are initially excessively high and decline to a lower, steadier value. The elevated values are due to the spark energy being high enough to over-drive the flame, a well-known experimental phenomenon [18]. It might be thought that over-driven flames would be avoided if the mixture were to be ignited by the minimum ignition energy. To do this involves extra complications and, as will be shown, this is not necessarily a rewarding undertaking. As a result, amounts of energy somewhat in excess of this are usually employed. This can result in over-driven flames with enhanced flame speeds that persist over a propagation distance that increases with the energy. Similarly, an ignition energy that is just in excess of the minimum can result in an under-driven flame, with a reduced flame speed that persists over an even greater propagation distance before it becomes fully developed.

The limit for the onset of a stable developed, stretched regime can be identified from separate plots of both flame speed against flame radius, as in Figs. 1-2, and, even more appropriately, from plots of flame speed against stretch rate, as in Figs. 3-4 for the same explosions. In all these figures the inner, high stretch rate, limit is indicated by #. All of these flames were initially over-driven. An example of the plot of flame speed against stretch rate for an under-driven flame is given in Fig. 5, with this limit again indicated by #.

The early stage of flame speed development has been studied by direct numerical simulations, with detailed CH_4-air chemical kinetics in [12] and [18]. Results, based on initiating hot pockets, eschewing the more complex spark models, were shown in [18] as trajectories of normalised flame speed plotted against K_ℓ. Plots for different ignition energies close to the minimum ignition energy showed the inner stretch rate limit for the onset of the linear relationship between S_n and α to be insensitive to these ignition energies, once ignition had occurred. The form of these curves is similar to the measured curve in Fig. 5. Similar simulations for H_2-air in [19] showed the inner stretch rate limit to decrease (and the associated radius to increase) with increase in Lewis number. The same effect can be observed in Figs. 3 and 4, where the former, for ϕ = 0.9, has the higher Lewis number and smaller stretch rates at the # points.

The outer break-points at which, the flames becomes unstable, with the development of a wrinkled cellular structure and an associated increase in flame speed, are more readily identified from the flame speed versus stretch rate plots, exemplified in Figs. 3 and 4. This outer, low stretch rate, limit is indicated by * on Figs. 1-4. The flames at 0.1 MPa remained stable throughout these measurements but, as the pressure increased and Markstein numbers decreased, the onset of instabilities occurred at lower stretch rates and stable, developed, flames existed over an ever-narrowing range of stretch rates.

Values of S_n, in the absence of any instability or perturbation due to ignition, will be indicated by S. Changes in S arise partly from the decreasing proportion of unreacted mixture within the flame thickness and principally, from the changing total flame stretch rate, α, calculated from Eq. (1). As α decreases, the former effect soon becomes negligible and S is given by the linear relationship:

$$S_s - S = L_b \alpha \,. \tag{2}$$

Here S_s is the flame speed at zero stretch rate. The equation yields values of the burned gas Markstein length, L_b, and the stretched flame speed, S, when linearly extrapolated to α =0, (r=∞), yields S_s. These values are independent of the isotherm chosen for the measurement of the flame speed [12]. Because the combustion is at constant pressure, the laminar burning velocity, u_ℓ, can be found from [12, 13]:

$$u_\ell = S_s(\rho_b/\rho_u), \tag{3}$$

in which ρ_b and ρ_u are burned and unburned gas densities. The critical radius, r_{cl}, at the outer break point, when divided by δ_ℓ, gives Pe_{cl}. Comparisons of Figs. 3 and 4 show the instability to develop earlier, at a higher value of α, at the higher ϕ of 1.2. It also developed earlier for both mixtures as the pressure increased.

It is both convenient and practical to define a stretched burning velocity, u_{nr}, which expresses the rate of *creation of completely burned gas* and excludes the changing amount of unburned gas within the flame thickness [12]. This is in contrast to a stretched burning velocity, u_n, based on the rate of *disappearance of unburned gas* at the temperature of T_u,

which depends upon the flame thickness. The effect upon u_{nr} of the flame stretch rate arising from both the aerodynamic strain rate and the flame curvature terms is given by:

$$\frac{u_\ell - u_{nr}}{u_\ell} = K_s Ma_{sr} + K_c Ma_{cr} \,. \tag{4}$$

Here K_s and K_c are Karlovitz stretch factors for aerodynamic strain rate and flame curvature. They are the product of the respective stretch rates, α_s and α_c, expressions for which are given in [12], and the chemical time δ_ℓ / u_ℓ, while Ma_{sr} and Ma_{cr} are the associated Markstein numbers. The two Markstein numbers have different values and the first term on the right is usually dominant.

Values of u_{nr} are found from *S*, in the absence of any unburned gas entrainment effects, from Eq. (10) in [13]. The Markstein lengths for the strain rate, L_{sr}, and flame curvature, L_{cr}, are found from ρ_u / ρ_b, L_b, and the Markstein lengths associated with u_n, again as in [13]. When normalised by the flame thickness, given by ν / u_ℓ, these lengths yield Ma_{sr} and Ma_{cr}.

3. Results and Discussion

3.1 Vapour pressure

Only burning velocities of gaseous mixtures were studied, as two phase mixtures behave quite differently [**20**]. This required the partial pressure of ethanol at ϕ to be less than the vapour pressure for the temperature and all the injected liquid to be evaporated. Different values of vapour pressure appear in the literature. For example, in [4], at 311K, the measured value is 20.28 kPa, while in [**21**] and [**22**], the values are 15.8 and 15.84 kPa, respectively. Observations of evaporation of the injected ethanol suggested the value was closer to those in [**21**] and [**22**] and values were taken from these sources.

3.2 Laminar burning velocity

The range of the measurements can be seen from Table 1, which gives the values of L_b. The measured values of u_ℓ at 358K and 0.1 MPa are indicated, with error bands, by the cross symbol and the solid curve in Fig. 6. Also shown are values previously measured values from [7-9] at the temperatures indicated on the figure. The present data give higher values than the previous measurements for the richer mixtures, otherwise they are close to those from [9]. Both of these sets of data contained allowances for flame stretch rate, as did those from the

counter-flow flames of [8]. There were no such allowances in [7], where the use of ionisation probes to measure flame speeds was possibly less accurate than high speed photography. The values from [7] were taken from Fig. 6 of that reference.

Shown in Fig. 7 is a comparison of the present values of u_ℓ for 358K, given by the solid curves, with those from [7], for 350K, at 0.5 and 0.7 MPa, over a full range of ϕ. Neither the absence of an allowance for flame stretch, nor the lower temperature in [7] can explain the differences in values. Present values of u_ℓ measured at 358K and at different pressures between 0.1 and 1.4 MPa are given in Fig. 8. Measurements could not be made with near-stoichiometric mixtures at initial pressures greater than 1.2 MPa, because the associated maximum explosion pressure was 8.5 MPa, close to the maximum safe working pressure of 9 MPa. The corresponding limiting values of ϕ at 1.2 and 1.4 MPa are indicated by the points B on the figure. Although the maximum value of u_ℓ at 0.1 MPa and 358K is significantly higher than that of iso-octane, reported in [13], the values of u_ℓ for ϕ=0.8 and 1.0 at 1.0 MPa and 358K are both slightly lower.

It is assumed that the variation of u_ℓ with pressure might be expressed by an empirical law of the form

$$u_\ell / u_{\ell d} = \left(p/p_d\right)^a \text{ at 358K, between the pressure limits in Fig. 8.} \qquad (5)$$

The suffix *d* indicates datum values at 0.1 MPa and 358K. Logarithmic plots of the data on Fig. 8 yielded the values of *a* for different values of ϕ in Fig. 9. These are given, along with their estimated error bands. The maximum error is ± 7.8%. At ϕ = 0.8 and 1.0 the values are slightly more negative than those for iso-octane-air in [13]. Also shown on Fig. 9 by the open triangle symbol are the values from [7], measured over a pressure range of 0.1 to 0.8 MPa at 350K. These are significantly smaller, numerically, than the present values and almost invariant with ϕ.

The present measured variations of u_ℓ with ϕ at 0.1 MPa, 300, 358 and 393K are given in Fig. 10. At 300K the values of vapour pressures in [21] and [22] indicate that not all the fuel is evaporated for values of ϕ greater than 1.2 at 0.1 MPa. This limiting value of ϕ is indicated by A on the figure. Also shown by the different symbols are data at higher

temperatures, extending to 500K, taken from [7-9]. The presently measured variations of u_ℓ with temperature were correlated by an assumed empirical expression:

$$u_\ell / u_{\ell d} = \left(T/T_d\right)^b \text{ at 0.1 MPa, between 300 and 393K, for } 0.8 \le \phi \le 1.2 \text{ in Fig. 10.} \qquad (6)$$

The suffix *d* indicates a datum value at 300K and 0.1 MPa.

Logarithmic plots of the data in Fig. 10 yielded the values of *b* for different ϕ given in Fig. 11, with a maximum error band of ± 6.4%. There is an appreciable decrease in the value of *b* with increase in ϕ. For iso-octane-air with ϕ = 0.8 and 1.0, the values of *b* are 1.1 and 1.0 [13], significantly lower than the values in Fig. 11. The present lean and stoichiometric values of *b* are quite close to those measured in [7] and [9]. The upper two full line curves in Fig. 10, labelled 453 and 480K were obtained from Eq. (6), with the present values of *b* from Fig. 11. The former curve is somewhat lower than the data points from [8], while the latter curve agrees well with the data from [9].

Values of u_ℓ from the chemical kinetic model in [8] are given by the dashed curve and from that in [10] by the dotted curve. However, at 300K, it is erroneous to assume the mixtures were completely gaseous for ϕ greater than 1.2, the limiting value at A. In general, the computed values are higher than the present experimental ones and the computed values in [8] tend to be higher than those in [10]. At higher pressures, but still at 300K, evaporation must be incomplete at even lower values of ϕ. At 0.18 MPa the upper value of ϕ for complete evaporation is 0.7 and at 0.2 MPa it is 0.6. This is relevant to the comparison of modelled and experimental data that appears in [10] for values of ϕ at 300K between 0.6 and 1.4 at 0.2 MPa.

3.3 Markstein numbers

The values of L_b in Table 1 were obtained from Eq. (2) in the regime of stable flame propagation, for all the present experimental conditions. These values decrease with increasing pressure and increasing equivalence ratio, eventually becoming negative. The decrease with ϕ is associated with a decreasing Lewis number, due to ethanol having a lower diffusivity relative to the mixture than oxygen. The richer mixtures were easier to ignite than the lean mixtures and when L_b was negative the rich flames burned faster when stretched.

Shown in Fig 12 are the variations of the strain rate Markstein number, Ma_{sr}, with ϕ, at the different pressures and an initial temperature of 358K, obtained as described in Section 1. Values of δ_ℓ $(=\nu/u_\ell)$ were obtained from the measured values of u_ℓ, with values of ν from the Gaseq code [23]. The irregularities in the curves are indicative of the errors in obtaining Ma_{sr} by this technique and error bands that can only be tentative are assigned on the figure. There is a significant decrease in Ma_{sr} with increasing pressure and the changes in Ma_{sr} with ϕ become greater as the pressure increases. Negative values of Ma_{sr}, associated with marked instability, appear at 0.5 MPa. As the pressure increases, the extent of the stable regime with a developed flame speed is reduced and, with it, the accuracy of determination of L_b and Ma_{sr}.

Figure 13 shows similar trends for Ma_{cr}. It is possible that the present technique, developed in [12], insufficiently differentiates between values of Ma_{sr} and Ma_{cr}, as it does not deal separately with the effects of aerodynamic strain rate and of flame curvature. Such a separation was possible in the computational studies of [12], which included spherical implosions with only a curvature stretch rate, and a stationary spherical flame with zero total stretch rate. This gave greater differences in the values of Ma_{sr} and Ma_{cr} for methane-air flames than the experimental values of [14], obtained from spherical explosion flames using the present methodology. Some influence of temperature upon both Ma_{sr} and Ma_{cr} at different ϕ and at atmospheric pressure is shown in Figs. 14 and 15, respectively. In both cases an increase in temperature from 358 to 395K increases the Markstein number, particularly for the richer mixtures.

3.4 Critical unstable Peclet numbers and Karlovitz stretch factors

Peclet numbers at the onset of flame instability, Pe_{cl}, are given at pressures between 0.5 and 1.4 MPa in Fig. 16, for different values of ϕ and at 358K. Values of Pe_{cl}, and the differences between them, decease as ϕ increases. On the basis of experimental results over a range of conditions, Gu et al. [14] have correlated Pe_{cl} in terms of Ma_{sr} by

$$Pe_{cl} = 177Ma_{sr} + 2177 \text{ for values of } Ma_{sr} \text{ between -5 and 10.} \quad (7)$$

This relationship is shown by the broken straight line in Fig. 17, where the present values of Pe_{cl} at 358K are plotted against Ma_{sr}. Equation (7) is only a very approximate guide and tends to give values that are somewhat higher than the present measured values. Nevertheless, it also approximated the values of Pe_{cl} for lean hydrogen-air mixtures in which, as in the present work, Ma_{sr} could become negative [24]. A best-fit curve to the present experimental points is given by:

$$Pe_{cl} = 1808.6 \exp^{0.103 Ma_{sr}} , \tag{8}$$

shown by the full line curve in Fig. 17.

Because a flame is stabilised by a sufficiently high stretch rate, a critical Karlovitz stretch factor, K_{cl}, expressed in terms of the critical total flame stretch rate, α_{cl}, seems to be a more rational criterion for flame instability than Pe_{cl}. Instabilities would develop for values of K_ℓ less than K_{cl}. The relationship between Pe_{cl} and K_{cl} is now developed. From Eq. (1), in the regime of stable flames but at the onset of instability, at radius r_{cl}, and also invoking Eq. (2):

$$\alpha_{cl} = \left(2/r_{cl}\right)S_n = \left(2/r_{cl}\right)\left(S_s - L_b\alpha\right). \tag{9}$$

With Eq. (3), this gives:

$$K_{cl} = \left(2/Pe_{cl}\right)\left(\rho_u/\rho_b\right)\left(1 + 2L_b/\delta_\ell Pe_{cl}\right)^{-1}, \tag{10}$$

where $K_{cl} = \alpha_{cl}\delta_\ell/u_\ell$, the critical Karlovitz stretch factor for the onset of instabilities.

Values of K_{cl}, derived for the present conditions at 358K from Eq. (10) are shown by the bold symbols for the different values of Ma_{sr} in Fig 18. Also shown by the cross symbols are data points for a variety of other fuel mixtures, taken from [16]. The best fit curve to the present data also is shown by the full line curve, given by

$$K_{cl} = 0.0075 \exp^{-0.123 Ma_{sr}} . \tag{11}$$

The correlation of Eq. (11) is no better than that of Eq. (8), in terms of the associated Coefficients of Determination, determined by square regression. Both have the same value of this coefficient of 0.73. Equation (11) and the use of K_{cl} seem, however, more rationally based than the use of Pe_{cl} .

The estimated error bands on Ma_{sr}, given in Fig. 12, must be born in mind for Figs. 17 and 18. Furthermore, as Ma_{sr} becomes more negative the flame stretch regime in which stable flames can occur becomes narrower and the determinations of Ma_{sr} and u_ℓ less accurate. For very negative values of Ma_{sr}, of about -10, the initial flame becomes unstable almost immediately [**24**]. This raises questions about the value of computing u_ℓ for stable, unstretched, flames if an appreciable stretch rate is required to stabilise them.

3.5 Stretch rate for flame extinction

Measurements of the extinction stretch rate are usually made in counter-flow burners [1]. The long spatial persistence of the under-driven flame, shown in Fig. 5, suggest it might be possible to measure the extinction stretch rate in under-driven explosions, at flame initiation rather than at flame extinction. At the point # in Fig. 5, the flame may not be fully established because the stretch rate is excessive. The highest stretch rate just before the flame has become established, might tentatively be taken as the extinction stretch rate. If it were to be any higher, a normal propagating flame would not be possible. For the flame in Fig. 5, with ϕ=0.8, 0.1 MPa and 358K, the extinction stretch rate was 260 s^{-1}, compared with the measured and computed values of about 500 s^{-1} and 330 s^{-1}, respectively, at 300K in [1]. Unfortunately, this was the only flame with pronounced under-driven characteristics.

Because of the possible utility of this analysis, it was applied to the under-driven iso-octane-air flames at different ϕ in Fig. 3 of [13]. The limiting maximum stretch rates at the onset of the linear regime, at 0.1 MPa and 358K, are listed in Table 2. Also tabulated are the measured and computed extinction stretch rates for counter-flow iso-octane-air flames from [1] at 0.1 MPa, but at 300K. The computed values are from a revised Davis and Law mechanism [25]. There is fairly good agreement between the two sets of experimental values up to ϕ=1.1, but the computed values up to this value of ϕ tend to be less than the measured ones.

4. Conclusions

Laminar burning velocities, Markstein numbers, and the critical Peclet numbers for the onset of flame instability have been measured at pressures up to 1.4 MPa and temperatures up to

393K, for gas phase ethanol-air mixtures. Measurements were made during the constant pressure combustion in a spherical explosion bomb with central ignition in the regime of a developed, stable, flame, between that of an under or over-driven ignition and that of an unstable flame.

At high pressures, the volume of ethanol injected into the bomb could be quite high and it was necessary to ensure it could all be evaporated. Failure to do so results in erroneous values of u_ℓ. At the lowest temperature of 298K vapour pressures were insufficient to create gas phase mixtures for values of ϕ greater than 1.2 at pressures of 0.1 MPa. The safe working pressure of the bomb limited the maximum values of pressure and temperature at which measurements could be made with the present technique to 1.4 MPa and 395 K.

At a pressure of 0.1 MPa and 358K the measured maximum values of u_ℓ were somewhat lower than those previously measured, but for rich mixtures they were higher. They also tended to be lower than previously computed values. Other comparative data were available at different temperatures at 0.1 MPa, but other data at higher pressures were sparse. Empirical expressions have been developed for the variations of u_ℓ with pressure and temperature. Markstein numbers tended to decrease with pressure an increase slightly with temperature. These changes were more pronounced for richer mixtures.

At the outer, unstable, limit empirical expressions have been derived for Pe_{cl} and, the perceived more rational, K_{cl}. At the inner limit an innovative attempt was made to measure extinction stretch rates at low ignition energies, at the limit of the early stage of under-driven flame propagation. Insufficient under-driven data were available for ethanol-air, but this approach seemed to be reasonably successful for iso-octane-air.

To compare the burning velocities of ethanol with those of the gasolines would require a specification of the gasoline, but a comparison was made with iso-octane. In general, the differences were not great, although the burning velocity of ethanol has a greater temperature dependence.

Acknowledgements

The authors thank the Egyptian Education and Culture Bureau and the University of Helwan for financial support of M. S. M.

References

1. A. T. Holley, Y. Dong, M. G. Andac, F. N. Egolfopoulos, Combust. Flame 144 (2006) 448-460.

2. D. Bradley, P. H. Gaskell, X. J. Gu, M. Lawes, M. J. Scott, Combust. Flame. 115 (1998) 515-538.

3. J. W. G. Turner, R. J. Pearson, B. Holland, R. Pec, “Alcohol-based fuels in high performance engines,” SAE Paper 2007-01-0056 (2007).

4. J. A. Pumphrey, J. I. Brand, W. A. Scheller, Fuel 79 (2000) 1405-1411.

5. D. Bradley, M. Lawes, C. G. W. Sheppard, Proc. Instn. Mech. Engrs. 214 Part C, (2000) 257-268.

6. Derek Bradley, R. A. Head, Combust. Flame 147 (2006) 171-184.

7. Ő. L Gülder, Nineteenth Symposium (International) on Combustion, The Combustion Institute (1982), 275-281.

8. F. N. Egolfopoulos, D. X. Du, C. K. Law, Twenty-Fourth Symposium (International) on Combustion, The Combustion Institute Pittsburgh, (1992). 833–841.

9. S. Y. Liao, D. M. Jiang, Z. H. Huang, K. Zeng, Q. Cheng, Applied Thermal Engineering 27 (2007) 374-380.

10. N. M. Marinov, Int. J. Chem. Kin. 31(3) (1999) 183-220.

11. A. S. Al-Shahrany, D. Bradley, M. Lawes, R. Woolley, "Measurements of laminar burning velocities in explosions and implosions in a spherical bomb," in: D. Bradley, D. Drysdale, V. Molkov (Eds.), *Proceedings of The Fourth International Seminar on Fire and Explosion Hazards*, FireSERT, University of Ulster, 2004, pp. 189-199.

12. D. Bradley, P. H. Gaskell, X. J. Gu, Combust. Flame 104 (1996) 176-198.

13. D. Bradley, R. A. Hicks, M. Lawes, C. G. W. Sheppard, R. Woolley, Combust. Flame 115 (1998) 126-144.

14. X. J. Gu, M. Z. Haq, M. Lawes, R. Woolley, Combust. Flame 121 (2000) 41-58.

15. D. Bradley, C. G. W. Sheppard, R. Woolley, D. A. Greenhalgh, R. D. Lockett, Combust. Flame 122 (2000) 195-209.

16. D. Bradley, M. Lawes, Kexin Liu, “Limiting flame stretch rates for flame instabilities and flame quenching,” in: D. Bradley, D. Drysdale, V. Molkov (Eds.), *Proceedings of The Fifth International Seminar on Fire and Explosion Hazards*, University of Edimburgh, 2008, to be published..

17. A. S. Al-Shahrany, D. Bradley, M. Lawes, R. Woolley, Proc. Combust. Inst. 30 (2005) 225-232.

18. D. Bradley, C. G. W. Sheppard, I. M. Suardjaja, R. Woolley, Combust. Flame 138 (2004) 55-77.

19. Zheng Chen, M. P. Burke, Yiguang Ju, Proc. Combust. Inst. 32 (2009) 1253-1260.
20. M. Lawes, Y. Lee, N. Marquez, Combust. Flame 144 (2006) 513-525.
21. Carl L. Yaws, Handbook of Vapour Pressure, Gulf Pub., London, 1994.
22. Phase change data of ethanol. 2008. [online]. [Accessed 6th June 2008]. Available from World Wide Web:
<http://webbook.nist.gov/cgi/cbook.cgi?ID=C64175&Units=SI&Mask=4#Thermo-Phase>
23. C. Morley, Gaseq Chemical Equilibrium Program, c.morley@ukgateway.net.
24. D. Bradley, M. Lawes, Kexin Liu, S. Verhelst, R. Woolley, Combust. Flame 149 (2007) 162-172.
25. S. G. Davis, C. K. Law, Twenty-Seventh Symposium (International) on Combustion, The Combustion Institute, (1998) 521-527.

Table and Figure Captions

Table 1. Schedule of experiments with measured values of L_b (mm).

Table 2. Values of extinction stretch rates for iso-octane-air at 0.1MPa, [13], at 358K, and [1], at 300K.

Figure 1. Variations of flame speeds, S_n, with *r*, at 358K, three different pressures and ϕ = 0.9. Limits of stable, developed flame indicated by # and *.

Figure 2. Variations of flame speeds, S_n, with *r*, at 358K, three different pressures and ϕ = 1.2 . Limits of stable, developed flame indicated by # and *.

Figure 3. Variations of flame speeds, S_n, with α, for the conditions of Fig. 1, ϕ = 0.9. Limits of stable, developed flame indicated by # and *.

Figure 4. Variations of flame speeds, S_n, with α, for the conditions of Fig. 2, ϕ = 1.2. Limits of stable, developed flame indicated by # and *.

Figure 5. Variations of flame speed, S_n, with α, for ϕ = 0.8 at 358K and 0.1 MPa, at low ignition energy. Inner limit of stable flame indicated by #.

Figure 6. Present values of u_ℓ at 0.1 MPa and 358K and values from [7] to [9] at given temperatures.

Figure 7. Present values of u_ℓ at 0.5 and 0.7 MPa and 358K, compared with those from [7] at 350K.

Figure 8. Present values of u_ℓ at 358K and pressures from 0.1 to 1.4 MPa. B indicates safe working pressure limitation .

Figure 9. Exponent *a* in Eq. (5) for the effect of pressure on u_ℓ at 358K.

Figure 10. Values of u_ℓ at 0.1 MPa. Three lower full line curves are present values at 300 to 393 K. A indicates limiting gas phase mixture. Two upper full line curves at 453 and 480K are from Eq. (6). Experimental values form [7-9] shown by symbols. Computed values shown by dashed [8] and dotted [10]curves.

Figure 11. Exponent *b* in Eq. (6) for effect of temperature on u_ℓ at 0.1 MPa .

Figure 12. Measured variations of Ma_{sr} with ϕ at different pressures, indicated in MPa, and 358K.

Figure 13. Measured variations of Ma_{cr} with ϕ at different pressures, indicated in MPa, and 358K.

Figure 14. Values of Ma_{sr} at 0.1 MPa and temperatures of 358 and 395K.

Figure 15. Values of Ma_{cr} at 0.1 MPa and temperatures of 358 and 395K.

Figure 16. Variations of Pe_{cl} with ϕ at 358K for different pressures.

Figure 17. Variations of Pe_{cl} with Ma_{sr} at 358K for different pressures. Equation (8) is the best fit to the present data points.

Figure 18. Values of $\boldsymbol{K} = K_{cl}$ at 358K, from Eq. (10), expressed in terms of Ma_{sr}. Cross symbol shows data for other mixtures from [16].

p (MPa)	T_u (K)	ϕ								
		0.7	0.8	0.9	1.0	1.1	1.2	1.3	1.4	1.5
0.1	300		2.37	1.89	1.3	1.15	1.09			
0.1	358	2.11	1.36	1.18	1.1	0.92	0.67	0.45	0.19	-0.14
0.1	395		1.56	1.2	1.28	1.09	0.95	0.73	0.52	0.29
0.2	358		0.77	0.59	0.52	0.38	0.37	0.33	0.14	
0.5	358	0.71	0.47	0.32	0.21	0.11	0.02	-0.03	-0.22	
0.7	358	0.52	0.27	0.22	0.09	-0.03	-0.07	-0.22	-0.04	
1.0	358	0.34	0.04	-0.1	-0.19	-0.25	-0.28	-0.31	-0.35	
1.2	358	0.27	0.02	-0.16						
1.4	358	0.25	-0.07							

Table 1. Schedule of experiments with measured values of L_b (mm).

ϕ	Experimental values s^{-1}		Computed values DL98 revised [**25**] s^{-1}
	[13]	[1]	[1]
0.7		150	
0.8	250	260	130
0.9	385	430	238
1.0	500	510	310
1.1	475	500	360
1.2	390	500	380

Table 2. Values of extinction stretch rates for iso-octane-air at 0.1MPa, [13], at 358K, and [1], at 300K.

.

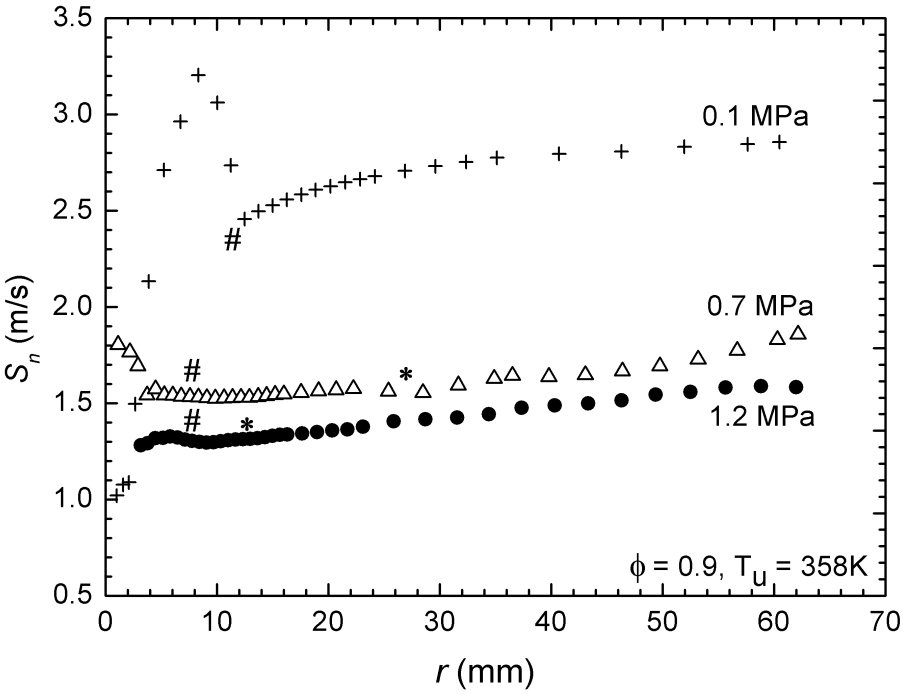

Figure 1. Variations of flame speeds, S_n, with *r*, at 358K, three different pressures and ϕ = 0.9. Limits of stable, developed flame indicated by # and *.

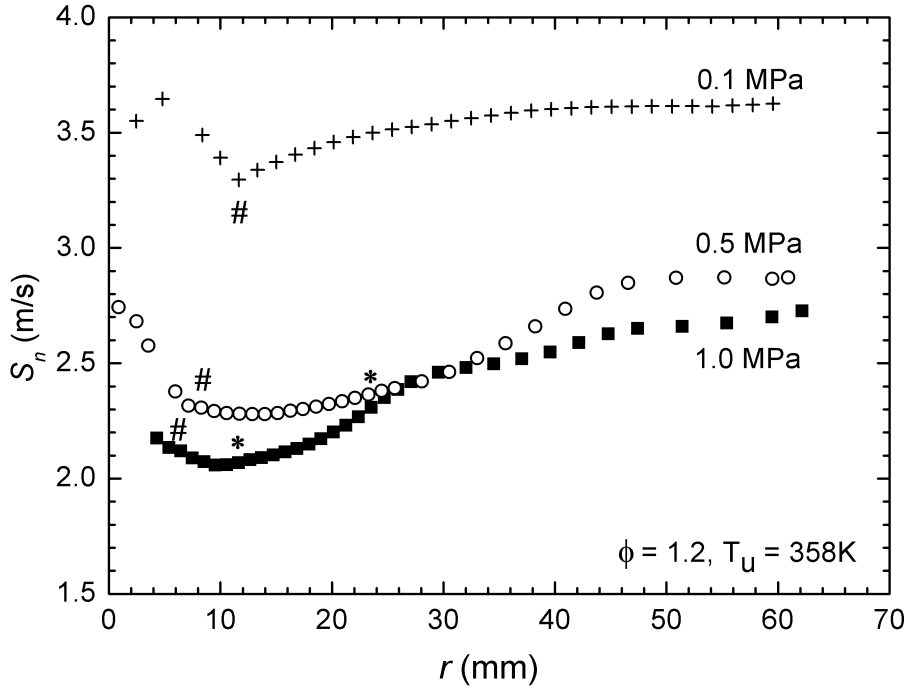

Figure 2. Variations of flame speeds, S_n, with *r*, at 358K, three different pressures and ϕ = 1.2 . Limits of stable, developed flame indicated by # and *.

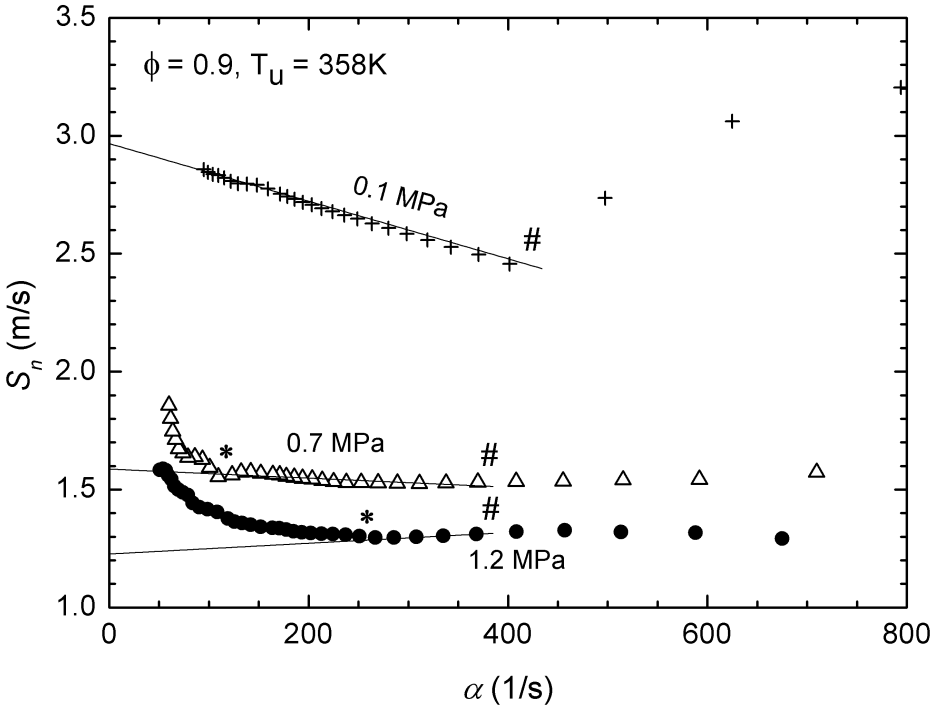

Figure 3. Variations of flame speeds, S_n, with α, for the conditions of Fig. 1, ϕ = 0.9. Limits of stable, developed flame indicated by # and *.

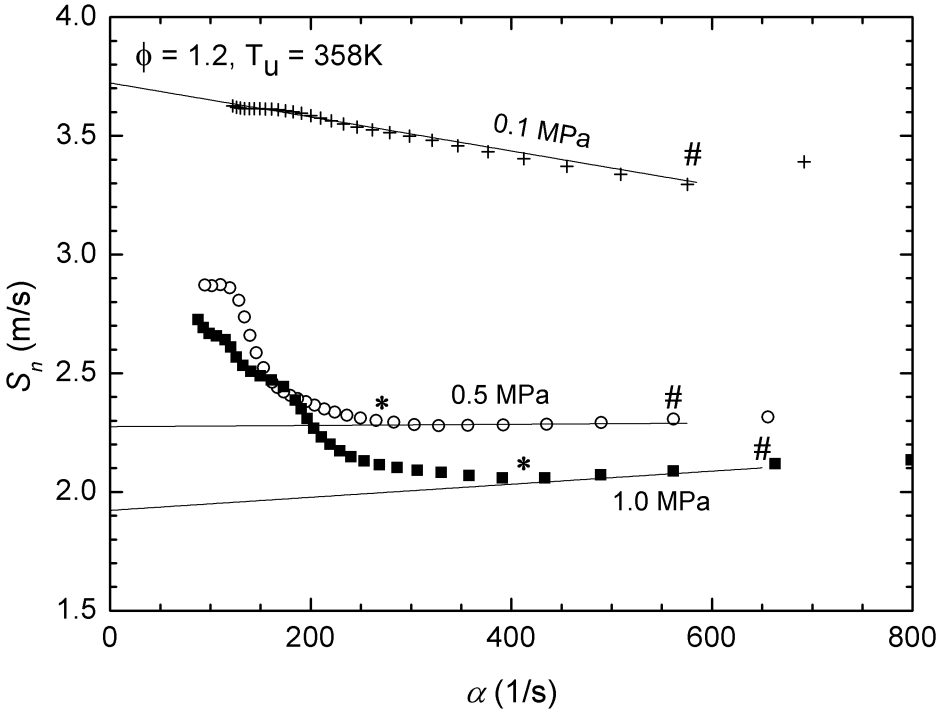

Figure 4. Variations of flame speeds, S_n, with α, for the conditions of Fig. 2, ϕ = 1.2. Limits of stable, developed flame indicated by # and *.

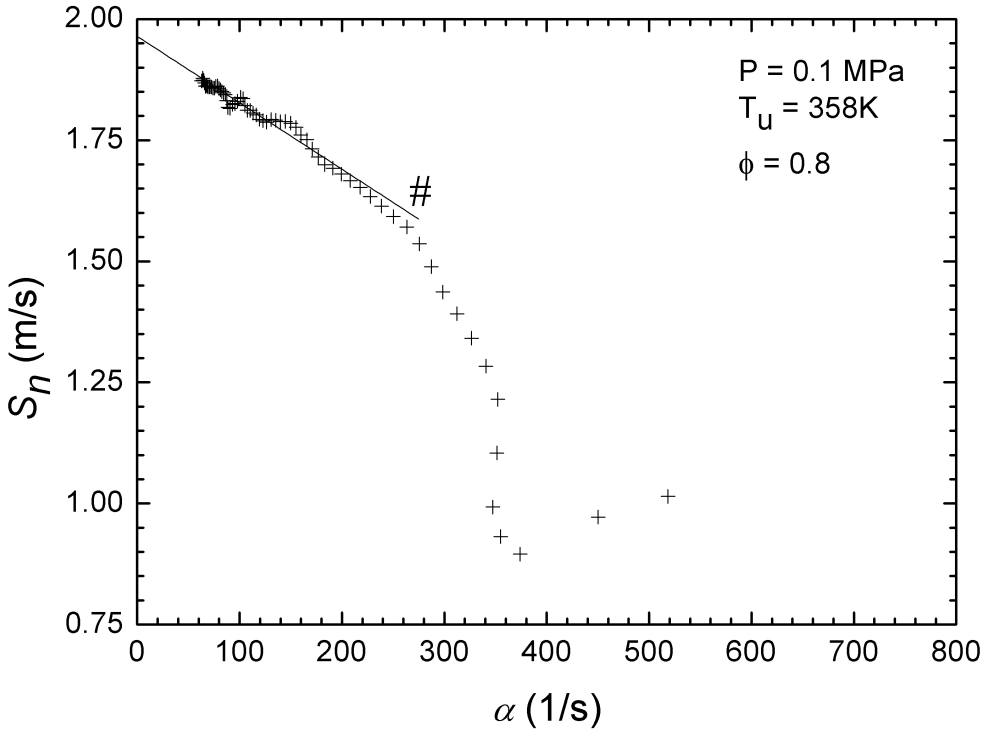

Figure 5. Variations of flame speed, S_n, with α, for ϕ = 0.8 at 358K and 0.1 MPa, at low ignition energy. Inner limit of stable flame indicated by #.

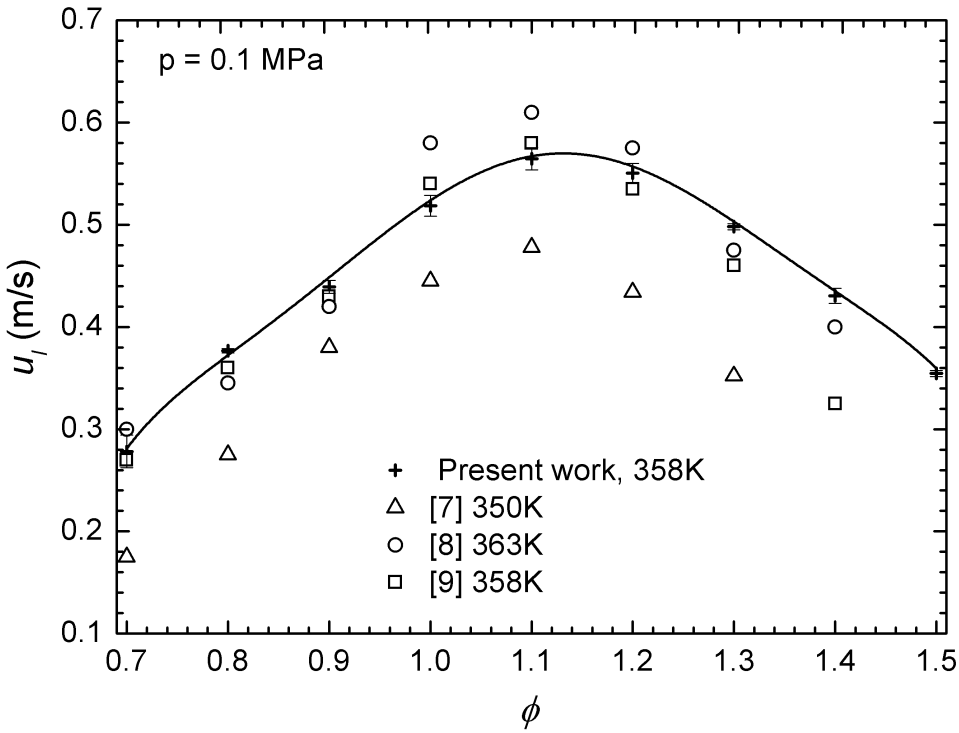

Figure 6. Present values of u_ℓ at 0.1 MPa and 358K and values from [7] to [9] at given temperatures.

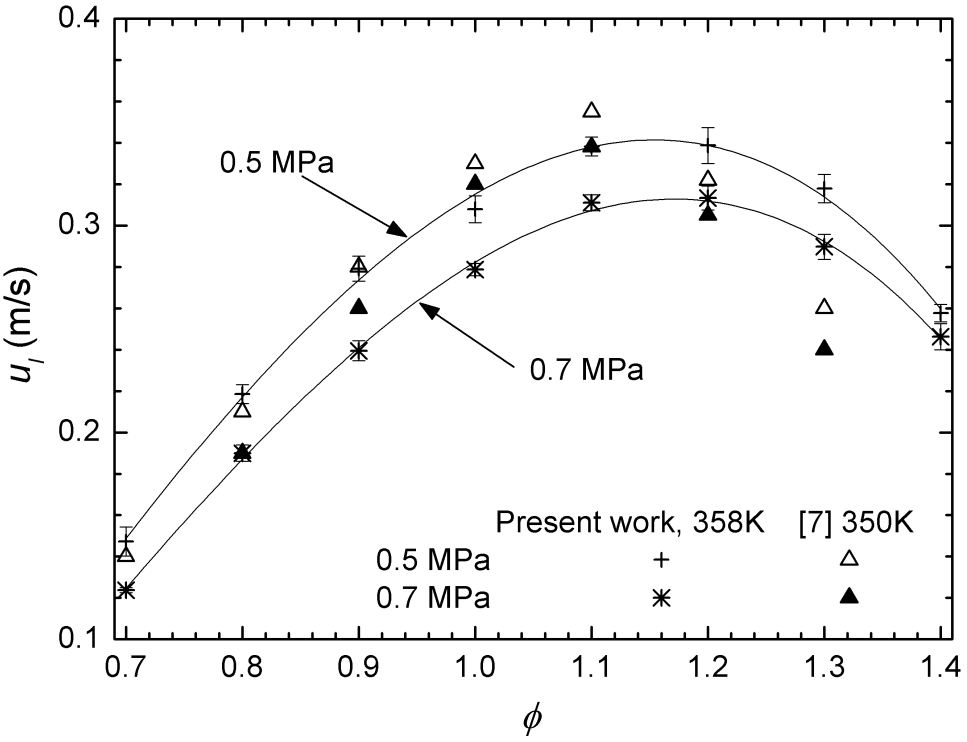

Figure 7. Present values of u_ℓ at 0.5 and 0.7 MPa and 358K, compared with those from [7] at 350K.

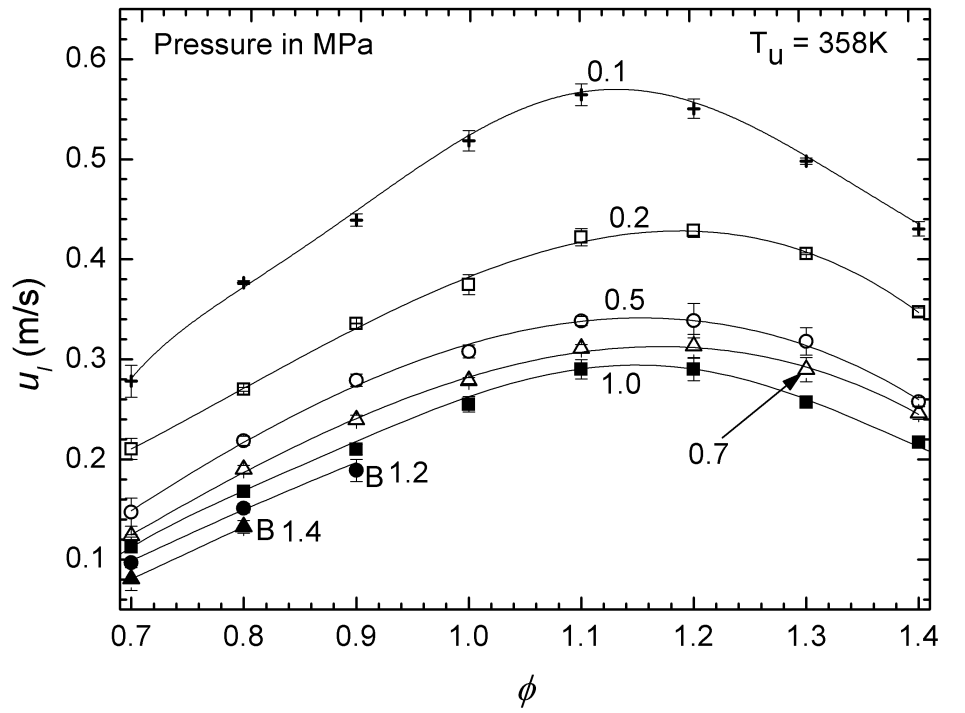

Figure 8. Present values of u_ℓ at 358K and pressures from 0.1 to 1.4 MPa. B indicates safe

working pressure limitation.

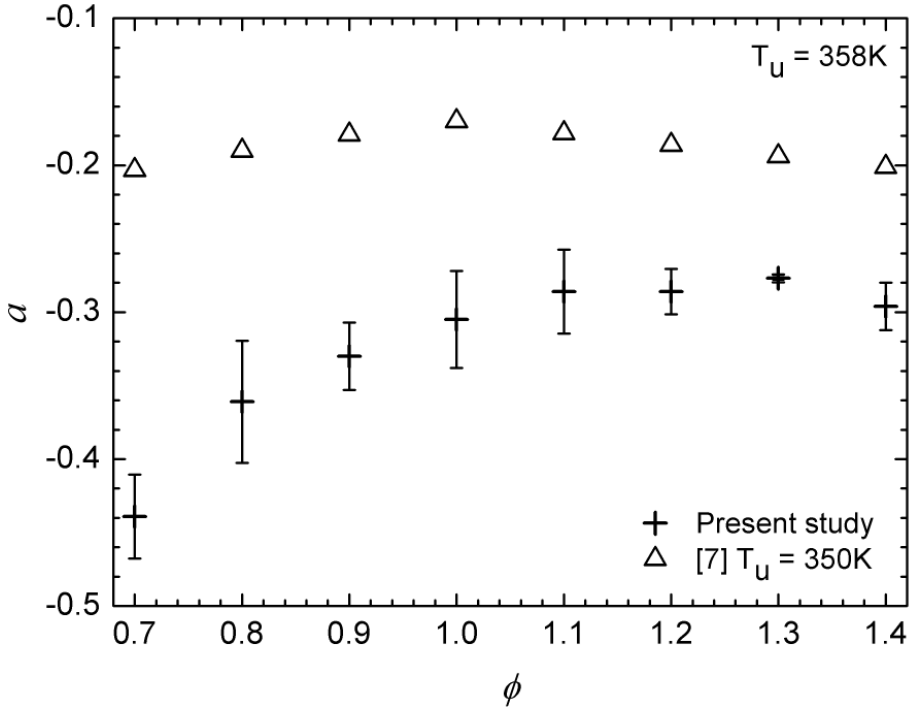

Figure 9. Exponent *a* in Eq. (5) for the effect of pressure on u_ℓ at 358K.

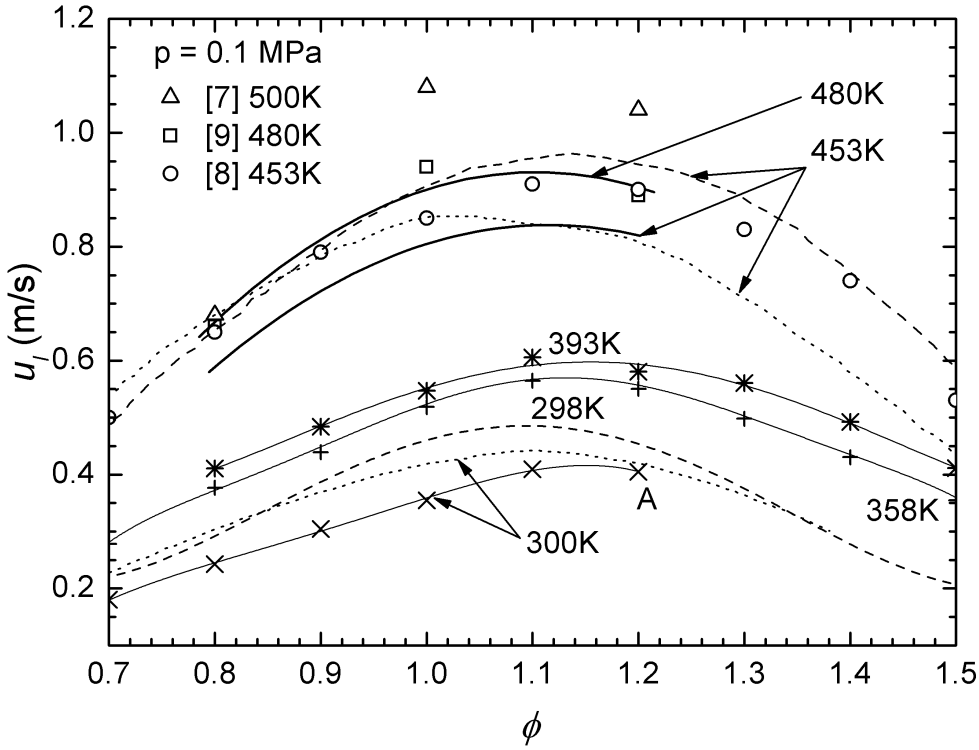

Figure 10. Values of u_ℓ at 0.1 MPa. Three lower full line curves are present values at 300 to 393 K. A indicates limiting gas phase mixture. Two upper full line curves at 453 and 480K are from Eq. (6). Experimental values from [7-9] shown by symbols. Computed values shown

by dashed [8] and dotted [10] curves.

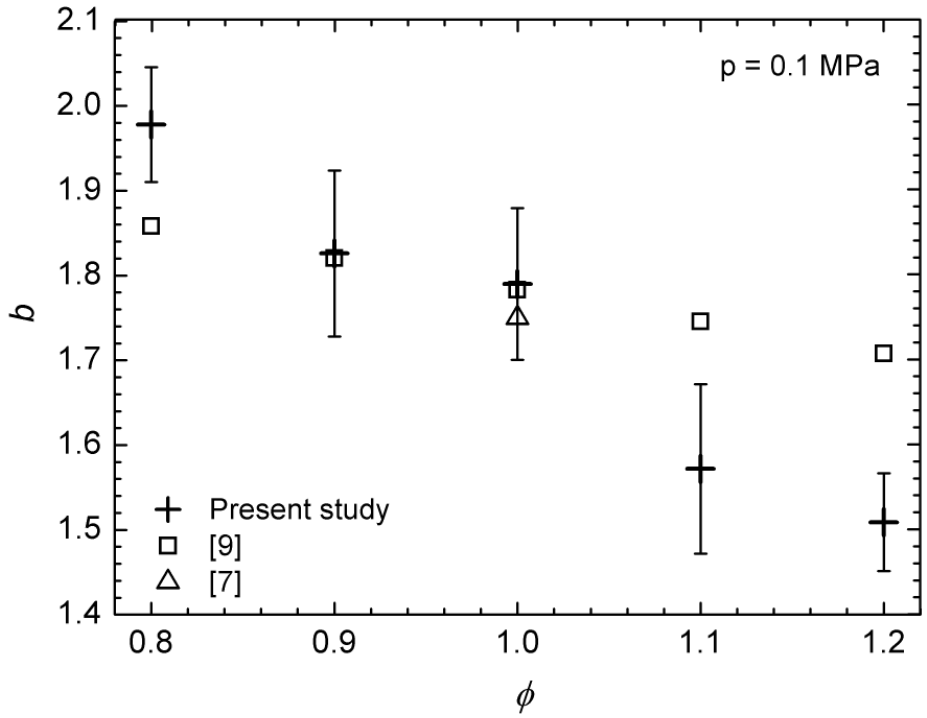

Figure 11. Exponent *b* in Eq. (6) for effect of temperature on u_ℓ at 0.1 MPa.

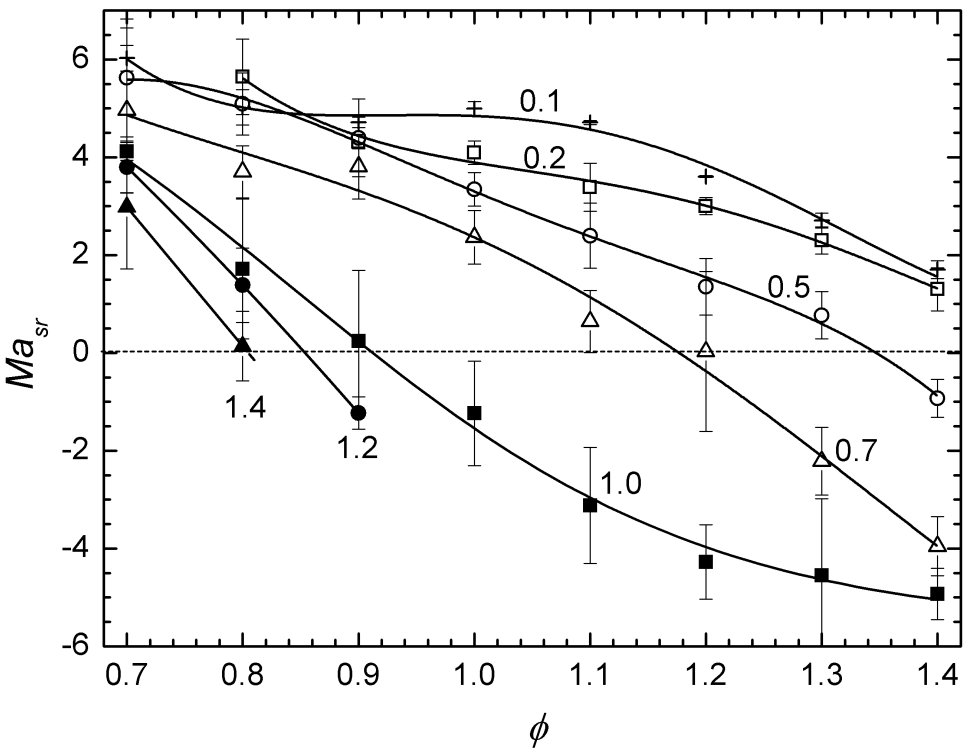

Figure 12. Measured variations of Ma_{sr} with ϕ at different pressures, indicated in MPa, and

358K.

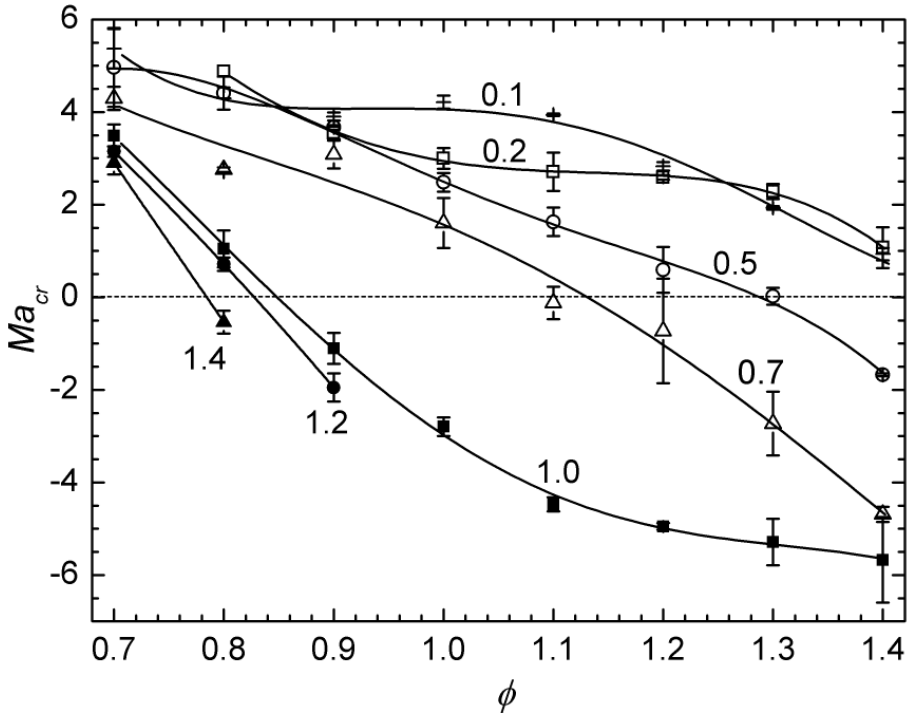

Figure 13. Measured variations of Ma_{cr} with ϕ at different pressures, indicated in MPa, and 358K.

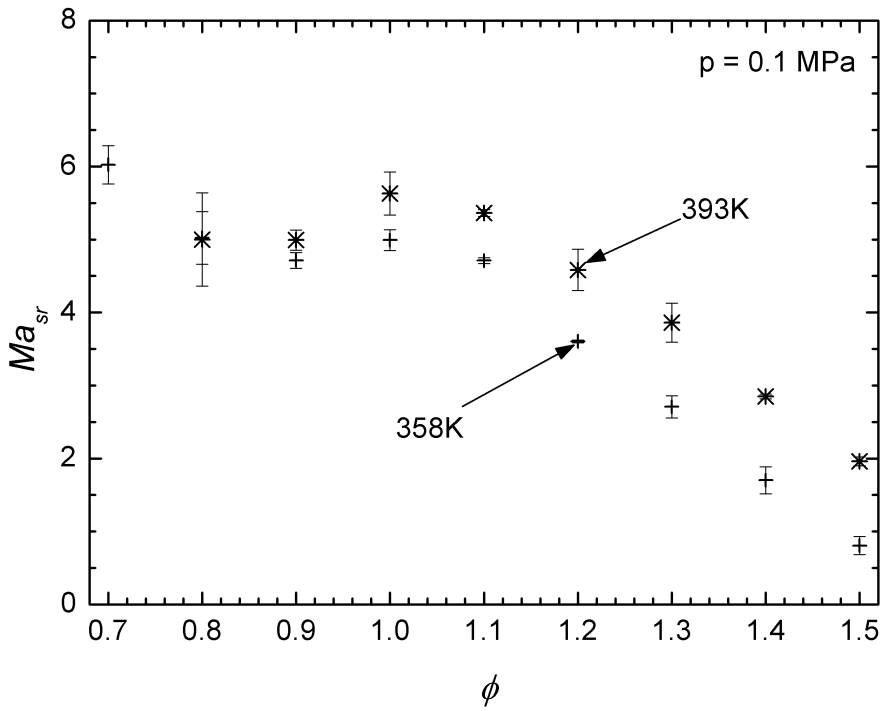

Figure 14. Values of Ma_{sr} at 0.1 MPa and temperatures of 358 and 395K.

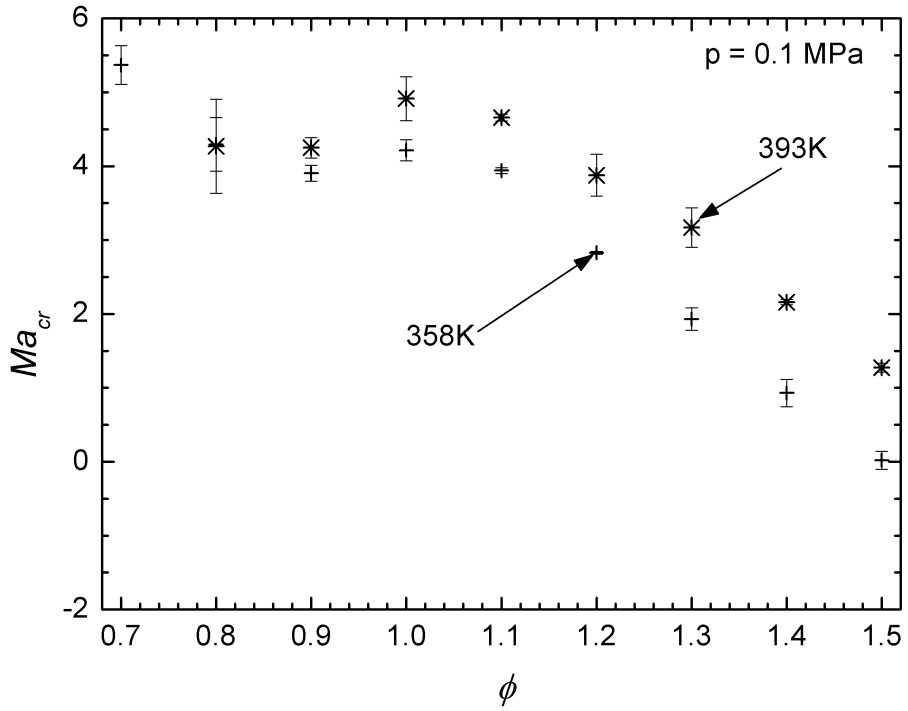

Figure 15. Values of Ma_{cr} at 0.1 MPa and temperatures of 358 and 395K.

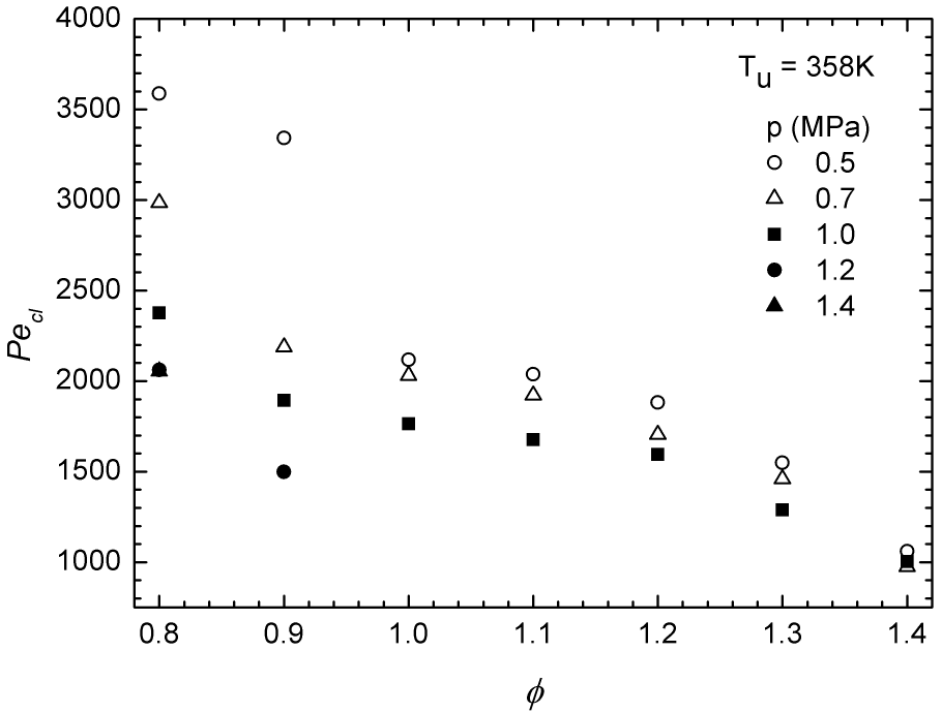

Figure 16. Variations of Pe_{cl} with ϕ at 358K for different pressures.

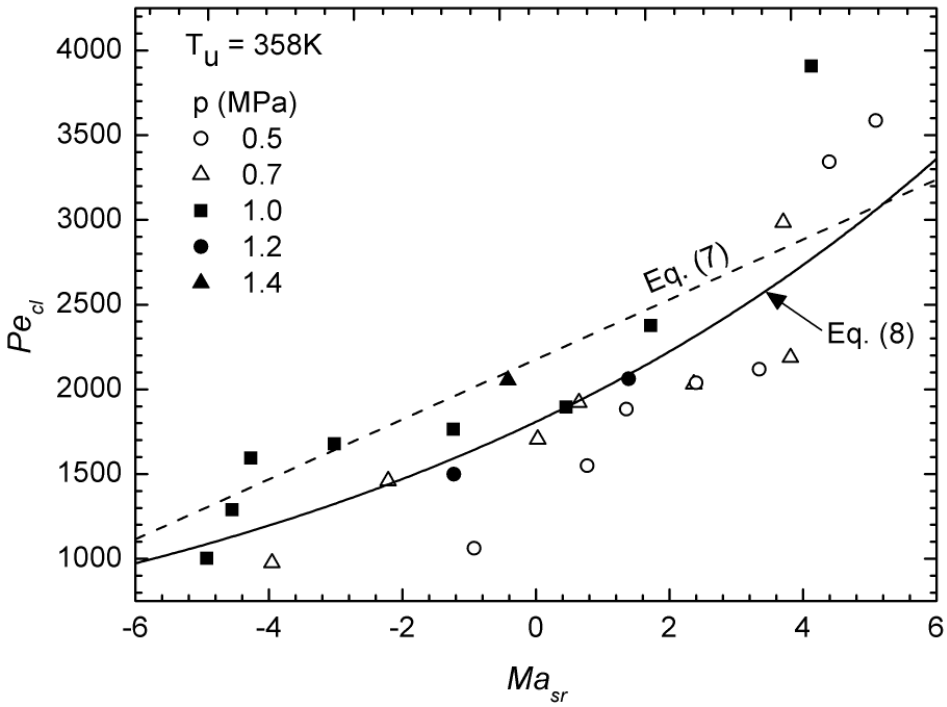

Figure 17. Variations of Pe_{cl} with Ma_{sr} at 358K for different pressures. Equation (8) is the best fit to the present data points.

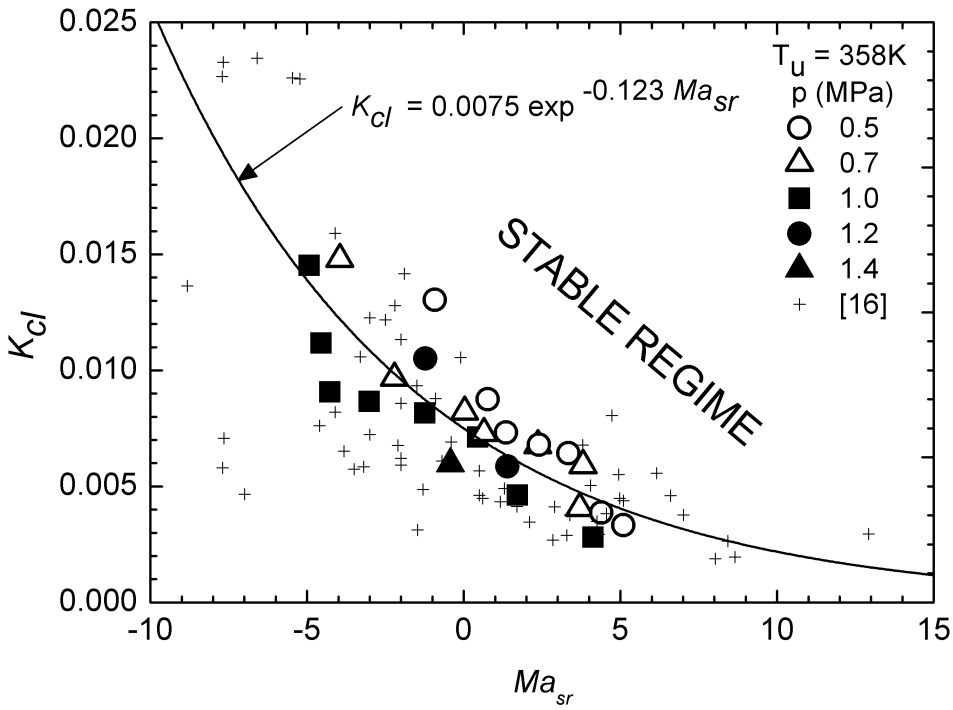

Figure 18. Values of $K = K_{cl}$ at 358K, from Eq. (10), expressed in terms of Ma_{sr}. Cross

symbol shows data for other mixtures from [16].